Opacity Effect on Extreme Ultraviolet Radiation from Laser-Produced Tin Plasmas

Shinsuke Fujioka,[1,*] Hiroaki Nishimura,[1] Katsunobu Nishihara,[1] Akira Sasaki,[2] Atsushi Sunahara,[3] Tomoharu Okuno,[1] Nobuyoshi Ueda,[1] Tsuyoshi Ando,[1] Yezheng Tao,[1] Yoshinori Shimada,[3] Kazuhisa Hashimoto,[3] Michiteru Yamaura,[3] Keisuke Shigemori,[1] Mitsuo Nakai,[1] Keiji Nagai,[1] Takayoshi Norimatsu,[1] Takeshi Nishikawa,[4] Noriaki Miyanaga,[1] Yasukazu Izawa,[1] and Kunioki Mima[1]

[1]*Institute of Laser Engineering, Osaka University, 2-6 Yamada-Oka, Suita, Osaka 565-0871, Japan*

[2]*Advanced Photon Research Center, Kansai Research Establishment, Japan Atomic Energy Research Institute, 8-1 Umemidai, Kizu, Kyoto 619-0215, Japan*

[3]*Institute for Laser Technology, 2-6 Yamada-Oka, Suita, Osaka 565-0871, Japan*

[4]*Department of Electrical and Electronic Engineering, Okayama University, 1-1 Naka 1-chome, Tsushima, Okayama 700-8350, Japan*

(Received 22 September 2005; published 29 November 2005)

Opacity effects on extreme ultraviolet (EUV) emission from laser-produced tin (Sn) plasma have been experimentally investigated. An absorption spectrum of a uniform Sn plasma generated by thermal x rays has been measured in the EUV range (9–19 nm wavelength) for the first time. Experimental results indicate that control of the optical depth of the laser-produced Sn plasma is essential for obtaining high conversion to 13.5 nm-wavelength EUV radiation; 1.8% of the conversion efficiency was attained with the use of 2.2 ns laser pulses.

DOI: 10.1103/PhysRevLett.95.235004 PACS numbers: 52.25.Os, 52.50.Jm, 52.70.La

Laser-produced high-Z plasma is a typical example of radiation hydrodynamics, in which the radiative properties of a plasma are tightly coupled with hydrodynamic motion via energy transport. A clear understanding of radiation hydrodynamics is important for the fields of inertial fusion energy [1], astrophysics and planetary physics [2], and x-ray source applications [3,4].

Extreme ultraviolet (EUV) light sources for microlithography are receiving much attention as an application of laser-produced high-Z plasma [5]. EUV lithography (EUVL) is a promising technology for volume production of next-generation microprocessors whose node size is less than 50 nm [6]. A commercial EUVL system requires 300 W of output EUV power into a solid angle of 2π steradian from a plasma source of 13.5 nm wavelength within a 2% bandwidth (BW). Laser-produced tin (Sn) plasma is an attractive 13.5 nm light source due to its compactness and high emissivity.

The opacity, as well as the emissivity, of laser-produced Sn plasma is so high for 13.5 nm light that the light emitted from deep within the Sn plasma is absorbed strongly during propagation through surrounding plasma as it expands [7]. To obtain high conversion efficiency (CE) from incident laser energy to output EUV energy, the plasma size should be controlled to attain an appropriate optical depth, i.e., the product of the mass absorption coefficient and area density of the plasma for 13.5 nm light. Recently the opacities of neutral through four-times ionized Sn have been reported [8]. These opacities are quite important for investigating EUV radiation transport in the low-temperature plasma periphery. The opacity of Sn plasma in the dominant EUV emission region is a critical parameter for investigating the optimum conditions for EUV generation; however, no reliable experimental data have been available. The electron temperature and ion density of the dominant EUV emission region are in the ranges from 20 to 80 eV and from 10^{17} to 10^{20} cm^{-3}, respectively [9,10].

Opacity measurements of Sn plasma were performed on the Gekko-XII laser facility [11]. Figure 1(a) shows the experimental setup for opacity measurement. A radiation-confining gold cavity, called the "dog bone " (DB), was used to uniformly heat an opacity sample [12]. The opacity sample consisted of a thin Sn layer sandwiched between two 1000 nm-thick CH tampers mounted on an observation window (200 μm $\times$ 200 μm) of the DB. The CH tamper was used to minimize the density gradient of the Sn plasma. The area density of the Sn layer in the sample was $2.04 \pm 0.18 \times 10^{-5}$ g/cm^2, which was analyzed with an inductively coupled plasma device.

Six beams of the Gekko-XII laser (1.053 μm wavelength, 500 ps pulse duration) were focused through two inlet holes of 500 μm diameter onto the inner surface of x-ray generation sections set at both ends of the DB. X-ray radiation from the sections propagated diffusively toward the central cavity for thermal radiation confinement. The DB was designed such that neither the reflected laser light nor the expanding laser plasma directly heated the sample. Moreover, x rays emanating from the laser plasma did not directly heat the sample.

The radiation temperature (T_R) in the central cavity was measured with a transmission grating spectrograph coupled with a cooled backillumination x-ray CCD camera. The absolute sensitivity of the spectrograph was separately measured. The spectrum and total energy of the thermal radiation through an observation window in the central body were fitted with the Planck function to derive T_R. Thermal radiation of T_R = 30–70 eV was generated

 © 2005 The American Physical Society

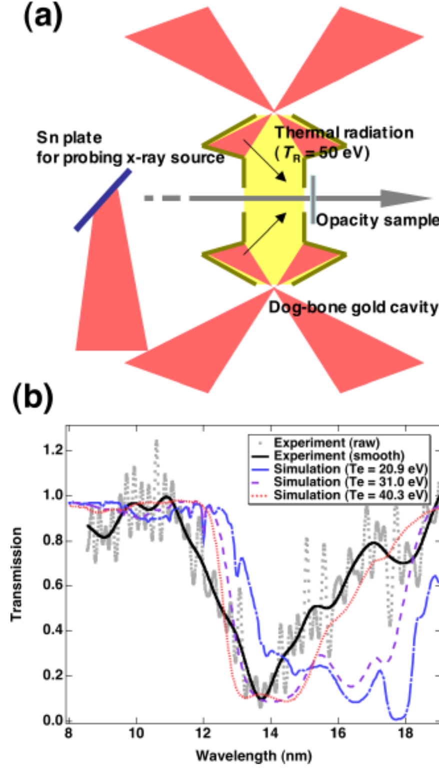

FIG. 1 (color online). (a) Experimental setup for opacity measurement. (b) Transmission spectra measured in experiment and calculated using the HULLAC code. The dots represent the raw spectrum measured in experiment, and the solid line is a smoothing of the experimental result considering the spectral resolution of the GIS-XSC. The dash-dotted, dashed, and dotted lines are the spectra calculated using the HULLAC code for electron temperatures of 20.9, 31.0, and 40.3 eV, respectively.

with a total incident laser energy of 50–1000 J according to the Stefen-Bolzmann equation.

The radiatively heated sample was backlit with broadband EUV light from another Sn plasma generated with a laser pulse of 1.053 μm wavelength and 500 ps duration at 1×10^{13} W/cm^2. The backlight source was set 2 mm away from the DB and backlight x rays were shone at 1.0 ns after the peak of the heating x ray. The transmitted EUV spectrum through the sample was measured by a grazing incidence spectrograph (GIS) coupled with an x-ray streak camera (XSC). A pair of grazing incidence total reflection mirrors coated with diamondlike carbon were set between the plasma and the GIS to filter out second-order diffraction light of wavelength less than 8 nm. A toroidal mirror was used to focus the backlight x rays into the 600 μm-width photocathode slit of the XSC.

The Sn sample was heated by a $T_R = 50$ eV thermal radiation pulse with a Gaussian shape (500 ps FWHM). Radiation-hydrodynamic simulation (ILESTA-1D) [13] predicts an averaged temperature and density of the heated Sn sample of 30 eV and 0.01 g/cm^3 at 1 ns after the peak of the heating x-ray pulse. For measuring the expansion velocity of the heated sample, an x-ray shadowgraph of the sample was observed from the side with a temporal resolved x-ray backlighting technique until 1.0 ns after the peak of the heating x-ray pulse. In this observation, the sample was backlit with Cu L-shell emission at 1.2 keV from a laser-produced Cu plasma. The expansion velocity derived from the observation ($3.8 \pm 1.1 \times 10^6$ cm/s) is consistent with that predicted (3.1×10^6 cm/s) by the ILESTA code.

Since the spectrum inevitably includes self-emission from the Sn and CH plasmas, we separately measured the self-emission spectra from the sandwiched Sn sample and from the CH tamper alone. In the self-emission measurement, the EUV backlight was switched off. Using four spectra, the pure transmission spectrum through only a Sn plasma was derived as

$$T(\lambda) = \frac{I_{\mathrm{Sn,abs}}(\lambda) - I_{\mathrm{Sn,self}}(\lambda)}{I_{\mathrm{CH,abs}}(\lambda) - I_{\mathrm{CH,self}}(\lambda)}, \quad (1)$$

where $I_{\mathrm{Sn,abs}}$ and $I_{\mathrm{Sn,self}}$ represent the intensity absorption and self-emission spectrum for the sandwiched Sn samples, and $I_{\mathrm{CH,abs}}$ and $I_{\mathrm{CH,self}}$ represent those for the CH tampers.

The dots in Fig. 1(b) represent the raw measured spectrum of the transmission, while the solid line in Fig. 1(b) is the smoothed measured spectrum in consideration of the spectral resolution of the GIS-XSC. The dash-dotted, dashed, and dotted lines represent the spectra calculated by an atomic code HULLAC [14] with electron temperatures of 20.9, 31.0, and 40.3 eV, respectively. The configuration interaction between the $4d^n$, $4d^{n-1}4f$, $4d^{n-1}5p$, $4d^{n-1}5f$, and $4p^5 4d^n$ configurations were taken into account, since the configuration interaction changes the wavelength and strength of emission lines considerably [15]. The population of the ionization state was calculated under the collisional radiative equilibrium condition. Strong absorption is seen around 13.5 nm, arising mainly due to the $4p$–$4d$ and $4d$–$4f$ transitions of Sn^{8+} to Sn^{13+}. Several dips seen between 15 and 18 nm are due to the $4d$–$4f$ and $4d$–$5f$ transitions of Sn^{4+} to Sn^{6+} ions. The transmission at 13.5 nm, the most interesting wavelength, shows quite good agreement between the measurement and calculation; however, there are some considerable discrepancies: (i) the calculated spectral width around 13.5 nm is broader than the experimental width; (ii) the short wavelength edge at 12.5 nm of the calculated spectra drops more sharply than that of the experimental spectrum; (iii) the wavelengths of some of the dips in the calculated spectra are different from those in the experimental spectrum. These disagreements may be rectified by taking more configuration interactions into account in the calculation, and this work is now in progress. Note again that the absorption cross section at 13.5 nm shows quite good agreement between the measurement and calculation, demonstrating that the HULLAC calculation is useful for optimizing 13.5 nm light generation. The measured mass absorption coefficient of the Sn plasma at 13.5 nm is $0.96 \pm 0.18 \times 10^5$ cm^2/g.

The opacity effect on the EUV emission from laser-produced Sn plasmas clearly appears as the size of the Sn plasma is changed. A second set of experiments was carried out using a Q-switched Nd:YAG laser focused with F/30 focusing optics at normal incidence with respect to the target surface. The laser intensity, spot size, wavelength, and pulse duration were fixed to be 1.0×10^{11} W/cm^2, 500 μm, 1.064 μm, and 10 ns, respectively. Sn-coated spherical plastic targets of 500 μm diameter were used with the Sn coat thickness varied from 10 to 50 nm. EUV spectra were observed with the GIS-XSC, which was installed at 45° from the laser incidence axis. The ablation thickness of a Sn layer was estimated to be from 30 to 50 nm under these experimental conditions [16], and therefore varying the Sn coat thickness is almost equivalent to changing the size and optical depth of the Sn plasma.

Figure 2(a) shows the spectra emitted from 10, 20, and 30 nm-thick Sn targets. It is obvious that the spectral shape broadens and the peak at 13.5 nm gradually flattens with increasing coat thickness. By subtracting two mutual EUV spectra for two different thicknesses, we can obtain the emission spectra of the corresponding Sn layer elements initially located at 0–10, 10–20, and 20–30 nm-depth in the target. As shown in Fig. 2(b), 13.5 nm light is emitted dominantly from the surface layer below the 10 nm-depth layer, while the emission spectra from above the 10 nm-depth layer have a flat top or even a dip structure and broad shape. The dip indicates that the expanding plasma strongly absorbs the 13.5 nm light emitted from the inside layer. The broad spectrum that is clearly observed in the EUV spectrum from the 20–30 nm-depth layer can be attributed to the satellite lines emitted from the multiply excited Sn ions and the opacity broadening during the radiation transport [17]. EUV emission was not observed from the layer located initially deeper than 30 nm, because Sn atoms in this layer were not sufficiently ionized to emit any EUV radiation. Laser energy transported into layers deeper than 10 nm is not efficiently converted into 13.5 nm light, and therefore only a thin Sn layer below 10 nm thickness should be heated by a laser pulse, giving efficient and narrow-band EUV emission.

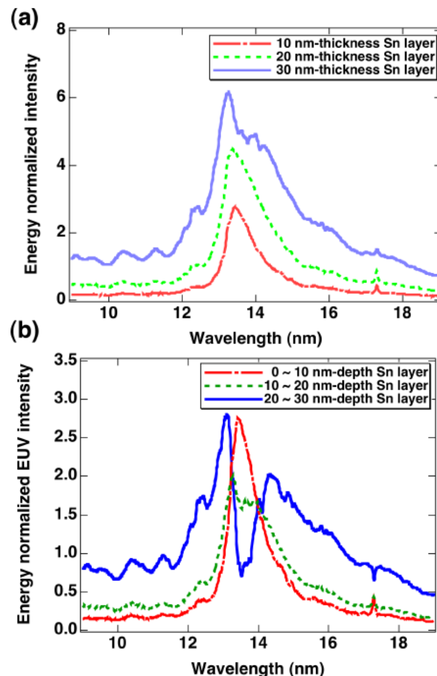

FIG. 2 (color online). (a) EUV spectra emitted from 10, 20, and 30 nm-thick Sn targets. (b) EUV spectra emitted from 0–10, 10–20, and 20–30 nm-depth Sn layers.

There are two well-known ways to control plasma size and optical depth. One method is to change the wavelength of the incident laser light [18,19]; shorter wavelength laser light heats higher density regions in the plasma, resulting in a larger plasma. The other method is to change the pulse duration of the incident laser light; longer duration laser pulse produces a larger plasma. The ablation thickness d_a (in centimeters) of a solid density Sn layer irradiated by 1.064 μm and 1.0×10^{11} W/cm^2 laser light is proportional to the pulse duration τ_L (in seconds): $d_a = 3.8 \times 10^2 \tau_L$ [16]. According to the scaling, a pulse duration of 2.6 ns is necessary to ablate a 10 nm-thick Sn layer.

We measured EUV-CEs with laser pulse durations of 2.2 and 8 ns. The CEs from the laser light into 13.5 nm light within a 2% BW emitted into 2π steradian were measured with an absolutely calibrated EUV calorimeter (E-mon of Jenoptik) [20]. The spectral response of the EUV calorimeter and the spectral shape and angular distribution of the EUV emission were taken into account for the CE evaluation.

Figure 3 shows EUV spectra from Sn plasmas produced by two laser pulses. The laser intensity was kept to 1.0×10^{11} W/cm^2. The spectra shown are normalized by the incident laser energy. The mass absorption coefficient measured in the opacity measurement is also plotted in Fig. 3 for comparison. In the case of the 8 ns pulse, a deep dip around 13.5 nm is clearly observed, while the dip disappears in the case of 2.2 ns laser pulse irradiation. This can be attributed to a shortening of the optical depth

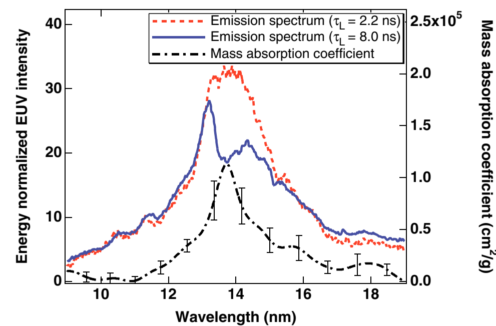

FIG. 3 (color online). Comparison of energy-normalized EUV emission spectra from Sn plasmas produced by 2.2 (dotted line) and 8 ns (solid line) laser pulses. The measured mass absorption coefficient of Sn plasma is also drawn (dash-dotted line) for comparison.

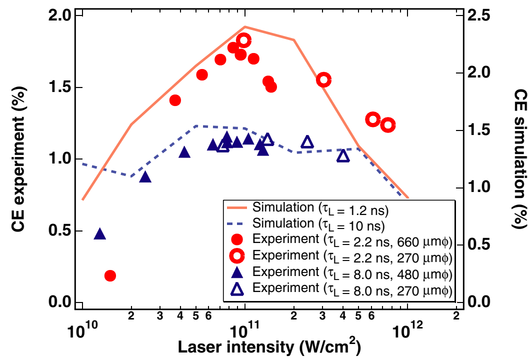

FIG. 4 (color online). Dependence of conversion efficiency from the incident laser into 13.5 nm radiation on the incident laser intensity and pulse duration. The solid and dotted lines are the predictions of one-dimensional radiation-hydrodynamic simulation. The circle and triangle points are experimental values. The open and closed marks distinguish the different laser spot sizes. Note that the left-hand scale applies to the experimental values and the right-hand scale to the predicted values.

of the Sn plasma. Good agreement between the wavelength of the dip and the peak of the absorption coefficient indicate that the measured opacity is highly relevant to the EUV generation.

The dip structure shown in Fig. 3 indicates that the produced plasma has a temperature gradient that decreases near the surface. The radiation flux at the center of the dip is practically equal to the Planck flux, which corresponds to $T_R = 25$ eV in the case of the 8 ns pulse and to $T_R = 29$ eV in the case of the 2.2 ns pulse. The effective surface temperature of the 8 ns pulse produced plasma is lower than that of the 2.2 ns pulse produced plasma probably due to multidimensional plasma expansion.

Figure 4 shows the dependence of the CE on incident laser intensity and pulse duration. For comparison, the predictions of a one-dimensional radiation-hydrodynamic simulation code (STAR) [7], which includes tabulated emissivities and opacities calculated by the HULLAC code, are also shown in Fig. 4 on a different scale. The open and closed marks represent different laser spot sizes. The experimental results show that a shorter pulse duration leads to a higher conversion efficiency. This trend is qualitatively consistent with the simulation. The maximum CE in the experiment is 1.8% at an intensity of 1.0×10^{11} W/cm^2 and 2.2 ns pulse duration.

There are two reasons why the experimental CEs are about 70% of the simulated values. The first reason is that experimentally produced plasma is not an ideal one-dimensional plasma, and lateral heat transport and plasma expansion along the target surface occurs in the plasma. The second reason is that EUV light emitted at an angle θ from the target normal should travel a distance $1/\cos\theta$ times longer in a plasma than that along the normal, and therefore the EUV absorption effect in the experiment is larger than in the calculation.

In summary, the absolute EUV absorption structure of Sn plasmas was measured for the first time. The experimental results indicate that control of the optical thickness is essential for obtaining efficient and narrow-band EUV emission due to its high emissivity and opacity; optically thinner plasma produced by shorter laser pulse emits 13.5 nm light more efficiently.

The authors would like to acknowledge valuable discussions on the opacity modeling with Dr. V. Novikov. We thank the technical support staff of ILE for laser operation, target fabrication, and plasma diagnostic. This work was performed under the auspices of a Leading Project promoted by MEXT (Japanese Ministry of Education, Culture, Sports, Science and Technology).

*Electronic address: sfujioka@ile.osaka-u.ac.jp

[1] J. Lindl, Phys. Plasmas **2**, 3933 (1995).
[2] F. J. Rogers and C. A. Iglesias, Science **263**, 50 (1994).
[3] I. C. E. Turcu and J. B. Dance, *X-rays from Laser Plasmas: Generations and Applications* (John Wiley & Sons, West Sussex, England, 1999).
[4] C. Rischel *et al.*, Nature (London) **390**, 490 (1997).
[5] F. Jin and M. Richardson, Appl. Opt. **34**, 5750 (1995); R.C. Spitzer *et al.*, J. Appl. Phys. **79**, 2251 (1996); A. Shimoura *et al.*, Appl. Phys. Lett. **75**, 2026 (1999); I.W. Choi *et al.*, J. Opt. Soc. Am. B **17**, 1616 (2000); Y. Shimada *et al.*, Appl. Phys. Lett. **86**, 051501 (2005); T. Aota and T. Tomie, Phys. Rev. Lett. **94**, 015004 (2005); P. Hayden *et al.*, Proc. SPIE-Int. Soc. Opt. Eng. **5751**, 919 (2005).
[6] W.T. Silfvast and N.M. Ceglio, Appl. Opt. **32**, 6895 (1993).
[7] A. Sunahara *et al.*, in *Proceedings of the 3rd International EUVL Symposium, Miyazaki, Japan, 2004* (International SEMATECH, Austin, TX, 2004).
[8] M. Lysaght *et al.*, Phys. Rev. A **72**, 014502 (2005).
[9] K. Nishihara *et al.*, in Proceedings of the 3rd International EUVL Symposium, Miyazaki, Japan, 2004 (Ref. [7]).
[10] Y. Tao *et al.*, Appl. Phys. Lett. **86**, 201501 (2005).
[11] C. Yamanaka *et al.*, IEEE J. Quantum Electron. **17**, 1639 (1981).
[12] K. Eidmann *et al.*, Phys. Rev. E **52**, 6703 (1995).
[13] H. Takabe *et al.*, Phys. Fluids **31**, 2884 (1988).
[14] A. Bar-Shalom, J. Oreg, and M. Klapisch, Phys. Rev. E **56**, R70 (1997).
[15] W. Svendsen and G. O'Sullivan, Phys. Rev. A **50**, 3710 (1994).
[16] S. Fujioka *et al.*, Proc. SPIE-Int. Soc. Opt. Eng. **5751**, 578 (2005); S. Fujioka *et al.* (to be published).
[17] A. Sasaki *et al.*, Appl. Phys. Lett. **85**, 5857 (2004).
[18] H. Tanaka *et al.*, Jpn. J. Appl. Phys. **43**, L585 (2004); Appl. Phys. Lett. **87**, 041503 (2005).
[19] M. Yamaura *et al.*, Appl. Phys. Lett. **86**, 181107 (2005).
[20] F. Bijkerk *et al.*, Technology Transfer 04024498A-TR, International SEMATECH Manufacturing Initiative, 2004 (http://www.sematech.org/docubase/abstracts/4498atr.htm).